Pharmaceutical Research, Vol. 26, No. 1, January 2009 (© 2008)
DOI: 10.1007/s11095-008-9707-z

Research Paper

Templated Open Flocs of Nanorods for Enhanced Pulmonary Delivery with Pressurized Metered Dose Inhalers

Josh D. Engstrom,[1] Jasmine M. Tam,[1] Maria A. Miller,[1] Robert O. Williams III,[2] and Keith P. Johnston[1,3]

Received March 14, 2008; accepted August 11, 2008; published online August 29, 2008

Purpose. A novel concept is presented for the formation of stable suspensions composed of low density flocs of high aspect ratio drug particles in hydrofluoroalkane (HFA) propellants, and for subdividing (templating) the flocs with aerosolized HFA droplets to achieve high fine particle fractions with a pressurized metered dose inhaler.
Methods. Bovine serum albumin (BSA) nanorods, produced by thin film freezing (TFF), were added to HFA to form a suspension. Particle properties were analyzed with an Anderson cascade impactor (ACI), static and dynamic light scattering and optical microscopy.
Results. The space filling flocs in HFA were stable against settling for one year. The pMDI produced high fine particle fractions (38–47%) with an emitted dose of 0.7 mg/actuation. The atomized HFA droplets break apart, that is template, the highly open flocs. Upon evaporation of HFA, capillary forces shrink the templated flocs to produce porous particles with optimal aerodynamic diameters for deep lung delivery.
Conclusions. Open flocs composed of nanorods, stable against settling, may be templated during actuation with a pMDI to produce optimal aerodynamic diameters and high fine particle fractions. This concept is applicable to a wide variety of drugs without the need for surfactants or cosolvents to stabilize the primary particles.

KEY WORDS: bovine serum albumin; floc; nanorod; pressurized metered dose inhaler; suspension stability.

INTRODUCTION

Until recently, the delivery of protein therapeutics has been largely limited to parenteral delivery due to the chemical and physical instabilities of proteins and challenges in permeating biological membranes (1). Among the non-invasive routes, pulmonary delivery offers advantages of large alveolar surface area (~100 m^2), rapid absorption across the thin alveolar epithelium (0.1–0.5 μm), avoidance of first pass metabolism, and sufficient bioavailabilities (1–8). For pulmonary delivery pressurized metered dose inhalers (pMDI) remain the most popular delivery device, relative to dry powder inhalers (DPI) and nebulizers, because of low cost, portability, and disposability (4,9). Because most drugs, including proteins, are insoluble in hydrofluoroalkane (HFA) propellants, most effort has focused on the design of stable suspensions (10–13), despite limited fundamental understanding (4,11,14). Although certain proteins in suspensions may potentially be denatured by HFAs (4), the low degree of contact in the solid state with the solvent, relative to solutions, is highly beneficial. For example, suspension-based pMDI formulations of insulin, lysozyme, catalase and rhDNase I have been shown to be stable (15–17).

To achieve high deposition of aerosolized particles in the deep lung, the aerodynamic diameter (d_a) should range between 1–5 μm (18). This size range may be produced by milling (11,17), spray drying (3,19–21), and spray freeze-drying (SFD) (22,23). Two recent particle engineering processes, spray freezing into liquids (SFL) (24–28), and thin film freezing (TFF) (29), were shown to produce high surface area, stable rod-like particles with 50–100 nm diameters and high aspect ratios, despite slower cooling rates than in SFD. The stability of lactate dehydrogenase, based on enzymatic activity, was increased in these processes relative to SFD, as a result of a reduction in the surface area of (26,29) the destabilizing gas–liquid interface (26,30). Limited process yields, in terms of weight of protein, for spray drying (50–70%) (22,31) and SFD (~80%) (22,31,32) are a major concern for highly valuable proteins.

To date, relatively few examples have been given of suspensions with 1–5% (*w*/*w*) mass loadings in HFAs that are stable against settling on time scales of over 60 s (11). To achieve high deposition of aerosolized particles in the deep lung, the aerodynamic diameter (d_a) should range between 1 and 5 μm (18). As the mass loading increases up to and above 5% (*w*/*w*), particles often aggregate within aerosolized droplets leading to unacceptably large d_a's. (11,33). Suspensions of cubic or spherical particles formed by milling or spray drying often flocculate irreversibly and settle in less than 60 s as illustrated in Fig. 1A (21). Settling can cause variable dosing between

[1] Department of Chemical Engineering, The University of Texas at Austin, Austin, Texas 78712, USA.
[2] Division of Pharmaceutics, College of Pharmacy, The University of Texas at Austin, Austin, Texas 78712, USA.
[3] To whom correspondence should be addressed. (e-mail: kpj@che.utexas.edu)

actuations (21,34). As a consequence of these limitations for pMDI suspensions, typical fine particle fractions (FPFs) only reach 5–30% (35). Although surfactants and cosolvents, such as ethanol, may stabilize the suspension, surfactants currently approved by the FDA for inhalation are insoluble in HFAs (36,37). Surfactant tails are often not solvated well enough by HFAs, which have low polarizabilities and van der Waals forces, to provide steric stabilization (38,39). Thus, a key goal has been to design new surfactant structures by achieving a fundamental understanding of the molecular interactions with atomic force microscopy and theory (11,38,39).

An alternative approach is to modify the particle morphology to enhance the colloidal stability of the primary particles (11,21,40). Large porous particles (40,41) or hollow particles with porous or nonporous shells (21) formed by spray drying were stable against settling for at least 4 hours when suspended in HFAs. Respirable fractions were as high as 68%. Here, the presence of pores filled with HFA decreases the density difference of the particle with the surrounding HFA media and reduces van der Waals attractive forces between particles (21,40,41). Recently, large porous nanoparticle (LPNP) aggregates, with d_a optimized for dry powder inhaler (DPI) delivery (20,33), have been formed by spray drying aqueous suspensions of submicron particles. Upon contact with lung tissue, these "Trojan particles" break up into nanoparticles to facilitate dissolution and absorption (20). To extend this approach to a pMDI, each LPNP could be stabilized as an individual entity in a colloidal dispersion. Efficient nanoparticle delivery to the deep lung has also been achieved with nebulization of nanoparticle dispersions in aqueous media (42). In all of the pMDI methods discussed so far, the goal has been to stabilize a colloidal dispersion of primary particles, or of individual LPNP particles in a HFA (11,14), in many cases with surfactant stabilizers.

The primary objective of this study was to produce aggregates of high aspect ratio particles, in this case nanorods, to achieve high fine particle fractions in pMDI delivery by: (1) forming stable (against settling) flocculated suspensions of bovine serum albumin (BSA) particles, (2) subdividing (templating) the friable flocs upon formation of HFA droplets, and (3) shrinking the flocs upon HFA droplet evaporation (Fig. 1). Here we purposely flocculate asymmetric high-aspect ratio particles without the use of surfactants or cosolvents in the HFA to prevent settling. Thus, this approach is fundamentally the opposite of most previous studies where pre-formed primary colloidal particles are stabilized in order to prevent flocculation (11).

The suspension stability and aerosol performance upon actuation from a pMDI was evaluated for BSA particles produced by TFF, wet milling and spray drying. The addition of cubes or spheres, produced by wet milling or spray drying, to HFA 227 produced dense flocs that settled rapidly (Fig 1A). In contrast, high aspect ratio particles, such as nanorods with 50–100 nm diameters produced by TFF, may be expected to pack less efficiently and form much lower density flocs with greater free volume (43–47) than spheres (Fig. 1B). These open flocs stack upon each other and occupy the entire vial to prevent settling for months, as illustrated in Fig. 1B. The morphology was determined by scanning electron microscopy (SEM) of the original particles and after solvent removal of particles suspended in HFA 227. Upon actuation of the pMDI,

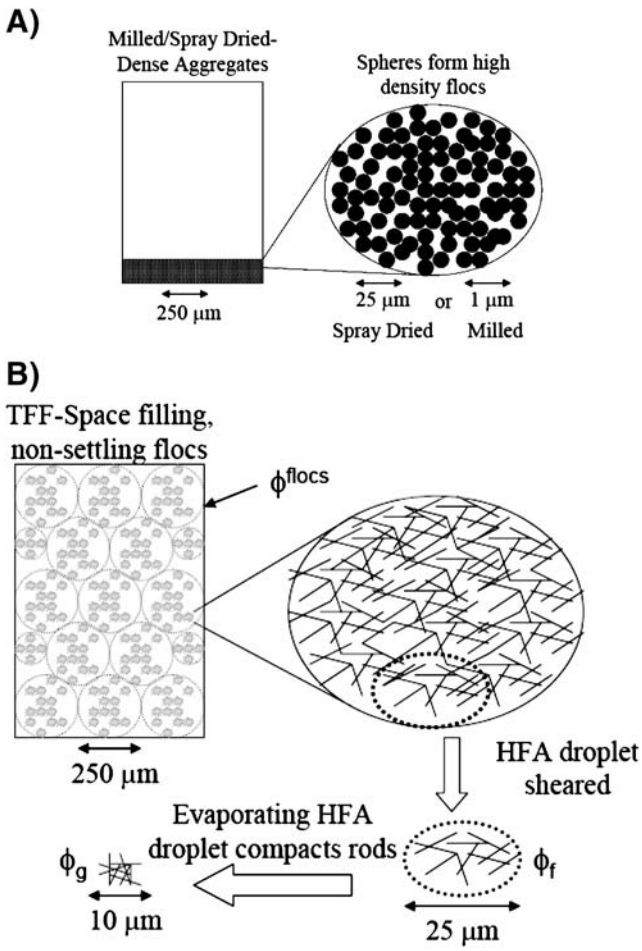

Fig. 1. Particle suspensions of milled or spray dried particles (**A**) and TFF rod particles (**B**).

the emitted HFA droplets were on the order of 25 μm. These 25 μm droplets subdivide and break apart the highly friable open flocs. We will define this process as "templating" of the flocs. Upon evaporation of the HFA droplet, the compression of the templated flocs from capillary forces will be shown to shrink the particles to produce a desirable d_a (Fig. 1B). The d_a values after actuation of the pMDI were determined with an Anderson cascade impactor (ACI) and aerodynamic particle sizer (APS) and geometric diameters of the aerosol particles (d_g) with SLS (static light scattering) and SEM micrographs.

In the discussion section, the mechanism of the particle formation is explored in detail. Experimental and calculated settling rates are utilized to characterize particle volume fractions and fractal dimensions for flocs composed of either cylindrical (rods) or spherical primary particles. Calculations of van der Waals energies between suspended particles are presented to explain floc formation and break up into subdomains upon templating the flocs with the HFA droplets. The calculated particle shrinkage during HFA evaporation from a material balance will be shown to agree with experiment.

THEORY

The formation of stable suspensions of purposely flocculated rods depends upon the ability of the open flocs to fill

large volumes in the vial. Experimental and theoretical studies indicate that rods create extremely low density flocs and thus fill much greater space compared to spheres as illustrated in Fig. 1A (44,46,47). For spheres, the volume fraction of primary particles within a floc ϕ_f is related to the floc diameter d^{floc}, primary particle diameter d_p, and fractal dimension D_f, which characterizes the floc structure, by (48)

$$\phi_f \approx \left(\frac{d^{floc}}{d_p}\right)^{D_f-3} \quad (1)$$

Philipse *et al.* modified Eq. 1 to account for the packing physics of cylindrical rods of length L and diameter D with the result (46)

$$\phi_f \approx \frac{1}{r}\cdot\left(\frac{d^{floc}}{V_p^{1/3}}\right)^{D_f-3} \quad (2)$$

where $r=L/D$ is the aspect ratio (46). A comparison of Eqs. 1 and 2 indicates that ϕ_f may be much smaller for particles with large aspect ratios as shown in Fig. 1 leading to flocs that fill a greater volume. Furthermore, if the attractive contact points of the rods prevent close packing during flocculation, the lower D_f for the rods will further reduce ϕ_f. These theoretical predictions will be demonstrated experimentally from microscopy, settling rates, and the aerodynamic and geometric diameters.

MATERIALS AND METHODS

Materials

Bovine serum albumin (BSA) was purchased from Sigma (St. Louis, MO, USA). The propellant 1,1,1,2,3,3,3-heptafluoroprane (HFA 227) was purchased from Hoechst (Frankfurt, Germany) and 2H,3H-Perfluoropentane (HPFP) was purchased from SynQuest Labs Inc. (Alachua, FL, USA). The Micro BCA Protein Assay Reagent Kit was obtained from Pierce (Rockford, IL, USA). The water was deionized by flowing distilled water through a series of 2×7 L mixed bed vessels (Water and Power Technologies, Salt Lake City, UT, USA) containing 60:40 anionic/cationic resin blends.

Powder Preparation

Thin Film Freezing (TFF)

BSA powders were prepared by the thin film freezing (TFF) process described previously (29). Briefly, 5 mg/mL feed solution of BSA in 10 mM pH=7.4 potassium phosphate buffer was passed at a flow rate of 4 mL/min through a 17 gauge (1.1 mm ID, 1.5 mm OD) stainless steel syringe needle. The droplets fell from a height of 10 cm above a rotating stainless steel drum (12 rpm) 17 cm long and 12 cm in diameter. The hollow stainless steel drum was filled with dry ice to maintain a drum surface temperature of 223 K. On impact, the droplets deformed into thin films and froze. The frozen thin films were removed from the drum by a stainless steel blade and transferred to a 400 mL Pyrex® beaker filled with liquid nitrogen. The excess liquid nitrogen was evaporated in a −80°C freezer.

A Virtis Advantage Lyophilizer (The Virtis Company, Inc., Gardiner, NY) was used to dry the frozen slurries. Primary drying was carried out at -40°C for 36 hrs at 300 mTorr and secondary drying at 25°C for 24 h at 100 mTorr. A 12-h linear ramp of the shelf temperature from −40°C to +25°C was used at 100 mTorr.

Spray Drying

Spray drying was performed with a Buchi Model 190 mini spray dryer (Brinkmann, Westbury, NY). A 10 mg/mL BSA feed solution in 10 mM potassium phosphate buffer (pH=7.4) was atomized using a 0.5 mm ID two fluid nozzle with an atomizing air flow rate of 200 mL/s. The liquid protein formulation was pumped through the nozzle by a peristaltic pump (VWR, Bridgeport, NJ) at a flow rate of 5 mL/min using 5 mm ID silicone tubing. The inlet temperature for the heated aspirator air was set to 150°C at a flow rate of 1,000 L/h. The resulting outlet temperature from the above conditions was 80°C.

Wet Milling

Bulk BSA powder as received was suspended at 5 mg/mL in acetonitrile. The BSA suspension was placed in a mill filled with 50 ceramic balls approximately 1 cm in diameter and milled on a mechanical roller for 24 h. The milled BSA suspension was dried in the Virtis Advantage Lyophilizer at a shelf temperature of 30°C for 12 h at 1000 mTorr.

Tapped Density

Approximately 100–300 mg of protein powder was loaded into a 100 mL graduated cylinder. The tapped density of the protein particles was measured with a Vankel tap density meter (Varian, Palo Alto, CA, USA).

Scanning Electron Microscopy

SEM images were collected on a Hitachi Model S-4500 scanning electron microscope (Hitachi Ltd, Tokyo, Japan). The samples were prepared in a dry-box. Aluminum stages fitted with double adhesive carbon conducting tape were gently dipped into sample vials until covered by powder. Stages were then placed in septum capped vials and purged with nitrogen for transfer. To minimize the time samples were exposed to atmospheric moisture the stages were rapidly transferred to a Pelco Model 3 sputter-coater. A conductive gold layer was applied and the samples were then quickly transferred to the SEM. Total exposure to the atmosphere was less than 1 min.

Preparation of HFA Suspensions

The various dried BSA powders were placed in 60 mL glass bottles (Qorpak, Bridgeville, PA, USA) and pre-cooled in a −80°C freezer. HFA 227 was also pre-cooled in a −80°C freezer and poured into the bottles containing the protein powders to form 0.7% (*w*/*w*) suspensions. The bottles were packed in dry ice and the suspensions were then sonicated for 2 min. using a Branson Sonifier 450 (Branson Ultrasonics

Corporation, Danbury, CT) with a 102 converter and tip operated in pulse mode at 35 W. Next, 10 mL of the cooled protein formulations were dispensed into 17 mL glass pMDI aerosol vials (SGD, Paris, France) and fitted with metering valves containing 100 μL metering chambers (DF10 RC 150, Valois of America, Inc., Congers, NY, USA). The vials were then allowed to warm up to room temperature.

Microscope Images of Protein Suspended in HPFP

The various particles were initially dispersed by pipette mixing in HPFP (~5 mg/mL) and were observed for 2 min. with a Nikon OPTIPHOT 2-POL optical microscope with an attached MTI CCD-72X camera (Nikon, Tokyo, Japan). Pictures were taken 30 and 60 seconds after initial dispersion in HPFP.

Particle Size Analysis

Particle sizes for the wet milled, spray dried and TFF particles were measured by static light scattering (SLS) with a Malvern Mastersizer-S (Malvern Instruments, Ltd.,Worcestershire, UK). Typical obscuration values ranged from 11 to 13%, corresponding to a BSA concentration of ~1 mg/mL.

Particle Size Analysis of Dried BSA Particles

The dried powders were first suspended in HPFP at a concentration of 5 mg/mL and sonicated for 2–3 min. Approximately 5 drops of the sonicated suspension were dispensed into a 15 mL vessel containing HPFP and a magnetic stir bar and the particle sizes were analyzed by SLS. The dried powders were also suspended in acetonitrile at a concentration of 5 mg/mL and sonicated for 2–3 min. Approximately 2 mL of the sonicated suspension was dispersed into a 500 mL acetonitrile bath and the particle sizes were analyzed by SLS.

Particle Size Analysis of TFF Particles Suspended in HFA

Vials containing TFF particles suspended in HFA 227 were cooled in a −80°C freezer. The metering valve was then removed from the vial and approximately 5 mL aliquots of the suspension were then dispensed into a 500 mL acetonitrile bath for particle size analysis.

Dynamic Light Scattering

Particles of BSA suspended in acetonitrile were analyzed by a custom-built dynamic light scattering (DLS) apparatus (49). The scattering angle was set to 90° and the data were analyzed using a digital autocorrelator (Brookhaven BI-9000AT) and a non-negative least-squares (NNLS) routine (Brookhaven 9KDLSW32). The suspension concentration was 0.5 mg/mL which gave a measured count rate of approximately 150 kcps. Measurements were made over a period of 2 min.

Moisture Content in Pressurized Metered Dose Inhalers

Moisture contents in the vials of each formulation were tested with an Aquatest 8 Karl-Fischer Titrator (Photovolt Instruments, Indianapolis, IN) according to the method described by Kim *et al.* (50). A 19 gauge needle was inserted through the septum of the titration cell with the needle tip placed below the reagent, and each formulation was measured in triplicate. For all formulations tested the moisture content was approximately 500 ppm. The pure HFA was found to have a moisture content of 250 ppm. The total amount of moisture to the amount of protein particles was 7% (*w*/*w*).

Optical Density Measurements of Protein

The μQuant spectrophotometer was used to measure turbidity at 350 nm to characterize BSA aggregation. Dry powders of BSA were reconstituted in 10 mM KPO_4 buffer (pH 7.5) to 1 mg/mL and 3×300 uL aliquots of each formulation were placed in a 96 well Falcon plate which was set in the spectrophotometer.

Quantitation of BSA

The amount of BSA was measured using the Micro BCA Protein Assay following protocols provided by Pierce (Rockford, IL, USA). Each sample was measured in triplicate with relative standard deviations (%RSD) <2%. The absorbance of the solutions was measured at 562 nm in a 96 well plate spectrophotometer (μQuant Model MQX200; Biotek Instruments Inc., Winooski, VT, USA). Untreated BSA was used to prepare the protein standards at concentrations between 2 and 30 μg/mL.

Dose Delivered Through the Valve (DDV) Determination

The protein suspensions in HFA were actuated once through the firing adaptor of a dosage unit sample tube (26.6 mm ID×37.7 mm OD×103.2 mm length; 50 mL volume; Jade Corporation, Huntingdon, PA, USA) (51). The firing adaptor was removed, and 40 mL of DI water was added to dissolve the protein. The sampling tube was shaken and allowed to sit for at least 30 min. to assure that the protein was dissolved in water. The protein concentration was determined using the Micro BCA protein assay in conjunction with the μQuant spectrophotometer. The glass vial containing the HFA protein suspension was weighed before and after each actuation to assure that the proper dose had been released. The measurement was repeated three times to get an average dose delivered through the valve (DDV) for each formulation.

Aerodynamic Diameter Characterization of Protein Aerosol

To characterize the aerodynamic properties of the particles, an eight-stage Anderson cascade impactor (ACI; Thermo-Anderson, Smyrna, GA) with an attached 15 cm spacer and an air flow-rate of 28.3 L/min was used to quantify mass median aerodynamic diameter (MMAD), geometric standard deviation (GSD), fine particle fraction (FPF), and emitted dose (ED). Initially 3 shots were sent to waste, and the next five shots were made into the ACI. The interval between shots was between 15–30 s to prevent cooling of the metering chamber and subsequent moisture condensation.

After the last dose was discharged, the glass vial was removed from the impactor and the valve stem and actuator were rinsed separately with a known volume of DI water. Each plate of the impactor was placed in a separate container with a known volume of DI water and soaked for 30 min. to assure complete dissolution. The protein concentrations were then measured with the Micro BCA Protein Assay.

The d_a of the protein particles were also determined in triplicate with an Aerodynamic Particle Sizer (APS) 3321 (TSI, Shoreview, MN, USA). The throat and spacer from the ACI were placed over the inlet of the APS and the airflow rate through the inlet was 5 L/min. Each formulation was shot once through the spacer and throat. The particle size range by mass was determined with the Aerosol Instrument Manager (AIM) software provided by TSI.

Geometric Diameter Characterization of Protein Aerosol

To obtain aerosolized particles for SEM (Hitachi Model S-4500, Hitachi Ltd) analysis, double carbon adhesive tape was applied to stage 3 of the ACI. Each formulation was actuated once through the ACI with an air flow rate of 28.3 L/min. The carbon tape was removed from stage 3 and applied to an aluminum SEM stage, which was transferred rapidly to a Pelco Model 3 sputter-coater to minimize exposure to moisture. Total exposure to the atmosphere was less than 1 min. The SEM micrographs were then characterized with imaging software (Scion, Frederick, MD) to determine the particle size distribution of at least 100 particles.

The aerosolized particles were also characterized by SLS. Each formulation was actuated once through the ACI spacer and throat. The aerosol exited the outlet of the throat downwards 5 cm directly above the laser beam of the Malvern Mastersizer S. For each formulation 100 measurements of the aerosolized spray were made every 5 ms. The recorded measurements were then averaged to give the final profile of the aerosolized particles on a volume basis.

RESULTS

Suspension Stability of the BSA Particles in HFA

Prior to forming suspensions of BSA in HFA 227, the morphologies of the dried BSA particles prepared by TFF, wet milling and spray drying were observed by SEM (Fig. 2). For BSA prepared by TFF, interconnected rods ~50–100 nm in diameter were observed with a web structure (Fig. 2A, B). Similar morphologies were observed previously for lysozyme produced by TFF at 223 K (29). The BSA particles prepared by wet milling (Fig. 2C) were in the form of cubes with 400–800 nm dimensions. Lastly, spray dried BSA at a feed concentration of 10 mg/mL produced spheres 3–6 μm in diameter with corrugated surfaces (Fig. 2D). Additionally, the bulk powder of the TFF particles before adding HFA had a low tapped density of 0.0064 g/cm^3 and required a mass of only ~100 mg to fill the entire volume of the vial (Fig. 2E). Alternatively, the same mass of dried wet milled and spray dried particles formed a thin layer at the bottom of the vial (data not shown).

The various dried BSA particles were suspended in HFA 227 at 0.70% (*w*/*w*) corresponding to a volume fraction in the vial ϕ_v of 0.0077 (Fig. 3), as determined from the true density of BSA ρ_p=1.3 g/cm^3 (52). For the TFF powder, the particles filled the entire volume of the vial immediately upon adding HFA (Fig. 3A) and did not settle even after 1 year in storage. For a control with an extremely low ϕ_v of only 0.070% (*w*/*w*; Fig. 3B) the TFF particles still filled approximately half the HFA volume. For the wet milled BSA particles, the suspension initially appeared to be uniform (like Fig. 3A), but the particles settled to the bottom after only 5 min (Fig. 3C). The spray dried particles dispersed well with shaking, but creamed after only 2 min (Fig. 3D).

Since the wet-milled particles settled in HFA 227 (1.41 g/cm^3) (53), >the wet milling raised ρ to above 1.3 g/cm^3. On the contrary, the wet milled particles creamed in HPFP (1.59 g/cm^3) (53). Thus, it was estimated that $\rho_p \sim 1.50$ g/cm^3, the average of the two solvent densities. Therefore, the true density reported for BSA appeared to be a skeletal density that did not account for internal pores. Upon wet milling removal of the pores raised ρ.

Characterization of the Flocs in a Surrogate Solvent HPFP at Ambient Pressure

Because the vapor pressure of HFA 227 is above ambient at 25°C (~500 kPa) (53), the flocs were not studied *in situ* by light scattering and microscopy. Instead, the particles were characterized at ambient pressure in HPFP, a surrogate nonvolatile solvent, with a similar polarity and polarizability as HFA 227(53–55). According to light microscopy, the TFF particles in HPFP were in the form of loosely packed flocs of rods (Fig. 4A and B). The rods formed 200–300 μm flocs with subdomains on the order of 25 μm within 5–30 s. after dispersing the particles by pipette mixing (Fig. 4A and B). The SLS measurements were consistent with the microscopy images in HPFP with $d(v,50)$ values between 215–259 μm (Fig. 5). For wet milled (Fig. 4C) and the spray dried (Fig. 4D) particles, 100 μm flocs formed in 30 seconds and grew to over 200 μm in 60 s. These flocs were more densely packed and composed of larger primary particles than those formed from TFF particles. About 50% of the wet milled particles by volume were between 1–10 μm with a secondary peak between 30–200 μm (Fig. 5). For the spray dried particles a single peak centered at 10 μm was observed (Fig. 5). The smaller sizes for light scattering *versus* microscopy may have been produced by shear from stirring.

Characterization of Particles Suspended in Acetonitrile

The various dried BSA particles were also suspended in a more polarizable solvent acetonitrile to gain fundamental knowledge about the dispersibility, primary particle size and flocculation properties. Upon suspending the particles in acetonitrile a milky uniform dispersion formed (Fig. 3E), but the particles settled after 3 days (Fig. 3F). The dispersion/settling behavior shown in Fig. 3E and F was also observed for wet milled and spray dried particles in acetonitrile (data not shown) with settling in ~3 days and ~30 min, respectively.

The BSA particles suspended in acetonitrile were also characterized by SLS after sonication for 2 min. As shown in Fig. 6 the $d(v,50)$ values were 330 nm, 410 nm and 6.3 μm for

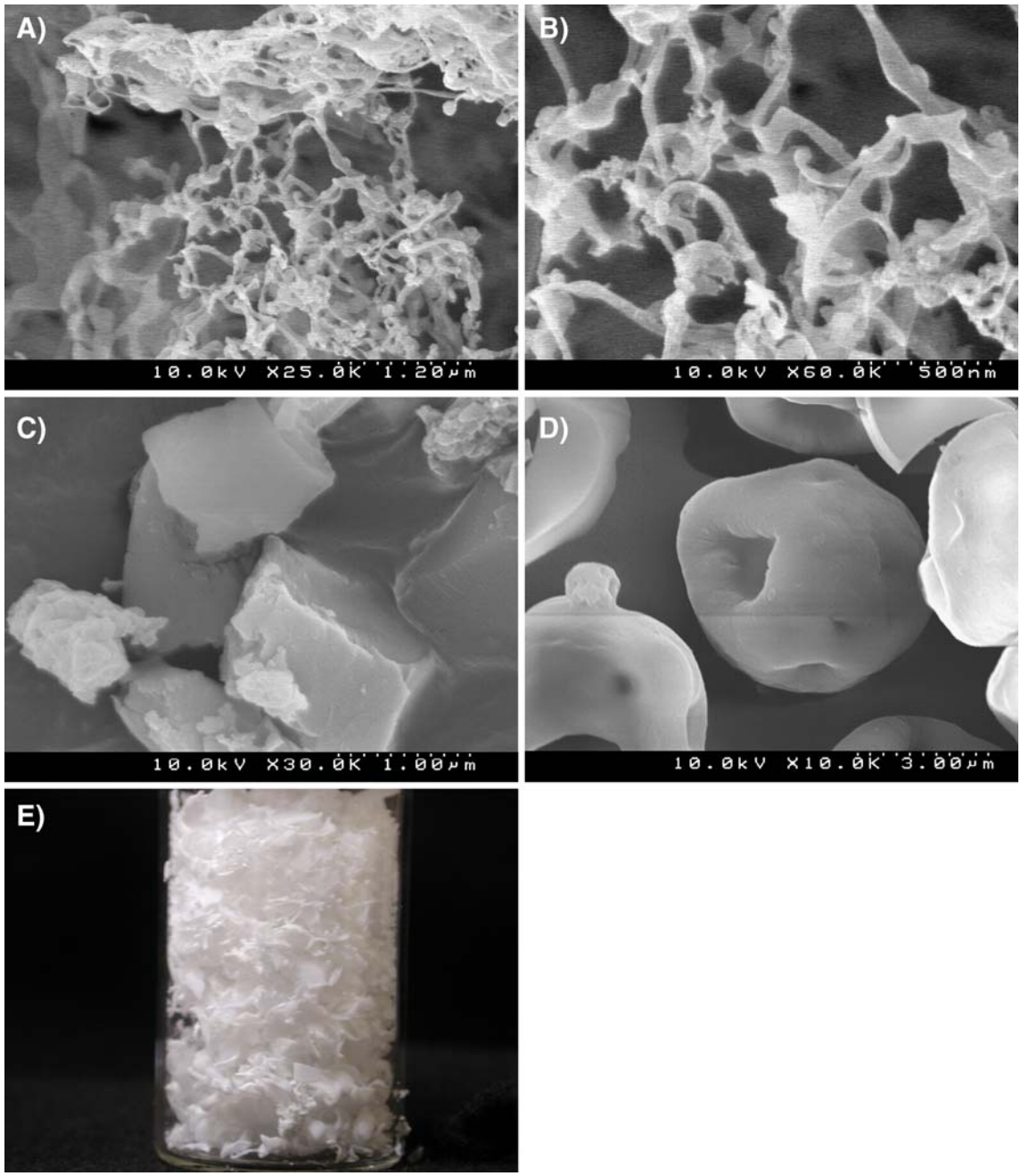

Fig. 2. TFF particles of BSA (**A**, **B** and **E**), milled BSA particles (**C**) and spray dried BSA particles (**D**).

the TFF, wet milled and spray dried BSA particles, respectively, consistent with the original sizes in the SEMs in Fig. 2. Even without sonication, significant dispersion of the TFF particles was observed with peaks at 330 and 20 µm, with approximately 50% of the particles by volume below 1 µm (Fig. 6). In SLS particle sizing results are based on the equivalent volume of a sphere. In the case of the TFF nanorods a measured particle diameter of 330 nm would have an equivalent volume of 0.019 μm^3. In the case of the nanorods with 100 nm diameters, the length of the rod would be 2.4 µm which is consistent with the SEMs in Fig. 2A and B. These experiments in acetonitrile demonstrated that the particles may be dispersed with little aggregation over 1 hr. to determine the primary particle size.

To determine if exposure of the TFF particles to acetonitrile caused morphological changes, the dispersions in ACN were frozen by drip freezing into liquid nitrogen. The acetonitrile was then removed by lyophilization leaving fluffy particles with an approximate tapped density of 0.012 g/cm^3 (Fig. 7A). When the particles were redispersed in acetonitrile the measured particle size profile was $d(v,50)=330$ nm which was similar to the profile in Fig. 6 of the original TFF dispersion, indicating the particles did not aggregate irreversibly. As observed by SEM, the morphology in Fig. 7B was 50–100 nm diameter rods, similar to the interconnected rods of the original TFF powder in Fig. 2A, and consistent with the sizes from light scattering results in Fig. 6. Thus exposure to acetonitrile does not alter the morphology significantly.

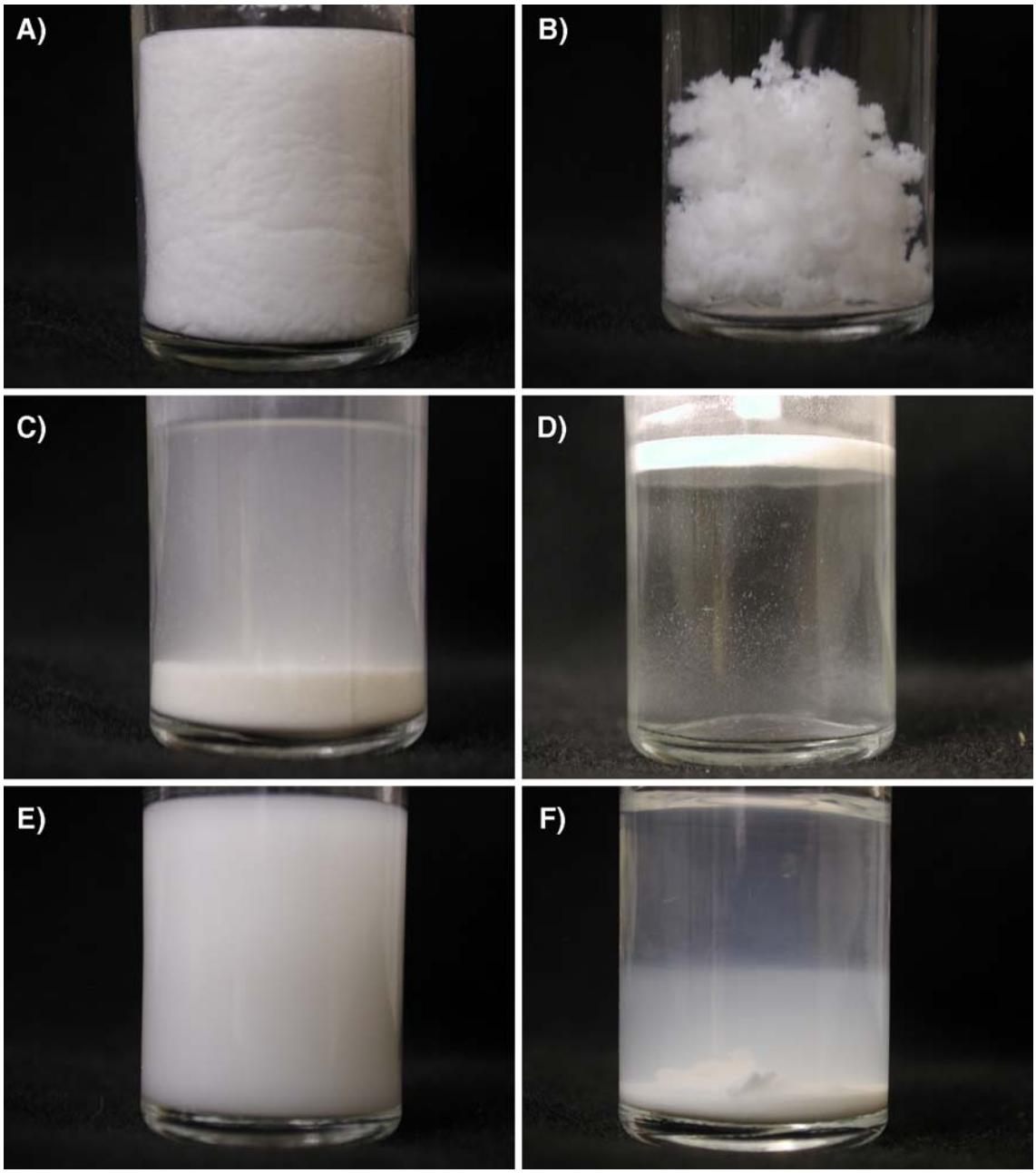

Fig. 3. Suspensions in HFA 227 of TFF particles at ϕ_v=0.0077 (**A**) and ϕ_v=0.00077 (**B**), wet milled particles 5 min after shaking (**C**) and spray dried particles at 2 min after shaking (**D**) at ϕ_v=0.0077, and TFF particles in acetonitrile at ϕ_v=0.0077 immediately after shaking (**E**) and 3 days after shaking (**F**).

TFF Particle Characterization after Recovery from HFA

To further understand the flocs of TFF particles in the HFA, the particles were characterized after HFA evaporation. Isolation of the particles from HFA by lyophilization could not be achieved since the freezing point (−131°C) of HFA 227 is too low to for conventional shelf lyophilizers (53,56). Alternatively, the HFA was cooled to -80°C, well below its boiling point of −16°C (53), and completely evaporated at atmospheric pressure. The TFF particle residue only occupied approximately 1 mL (tapped density of 0.10 g/cm^3, Fig. 8A), an order of magnitude less than that of the starting TFF bulk powder (Fig. 2E). The particle morphology after HFA exposure resembled rods with 100 nm diameters (Fig. 8B), similar to the original TFF particles in Fig. 2A. Therefore, exposure to HFA 227 followed by sonication did not significantly alter the primary nanorod particle morphology. However, the densified aggregates of the nanorods formed by capillary forces upon evaporation (Fig. 8A) of HFA were not redispersible when reintroduced into HFA or into acetonitrile.

A second approach was used to harvest the TFF particles from HFA for further characterization at ambient pressure. A 2 mL aliquot of the cold TFF suspension was mixed directly with 500 mL of acetonitrile at 25°C. The suspensions were sonicated and analyzed by SLS. The flocs deaggregated nearly completely to individual primary particles with over

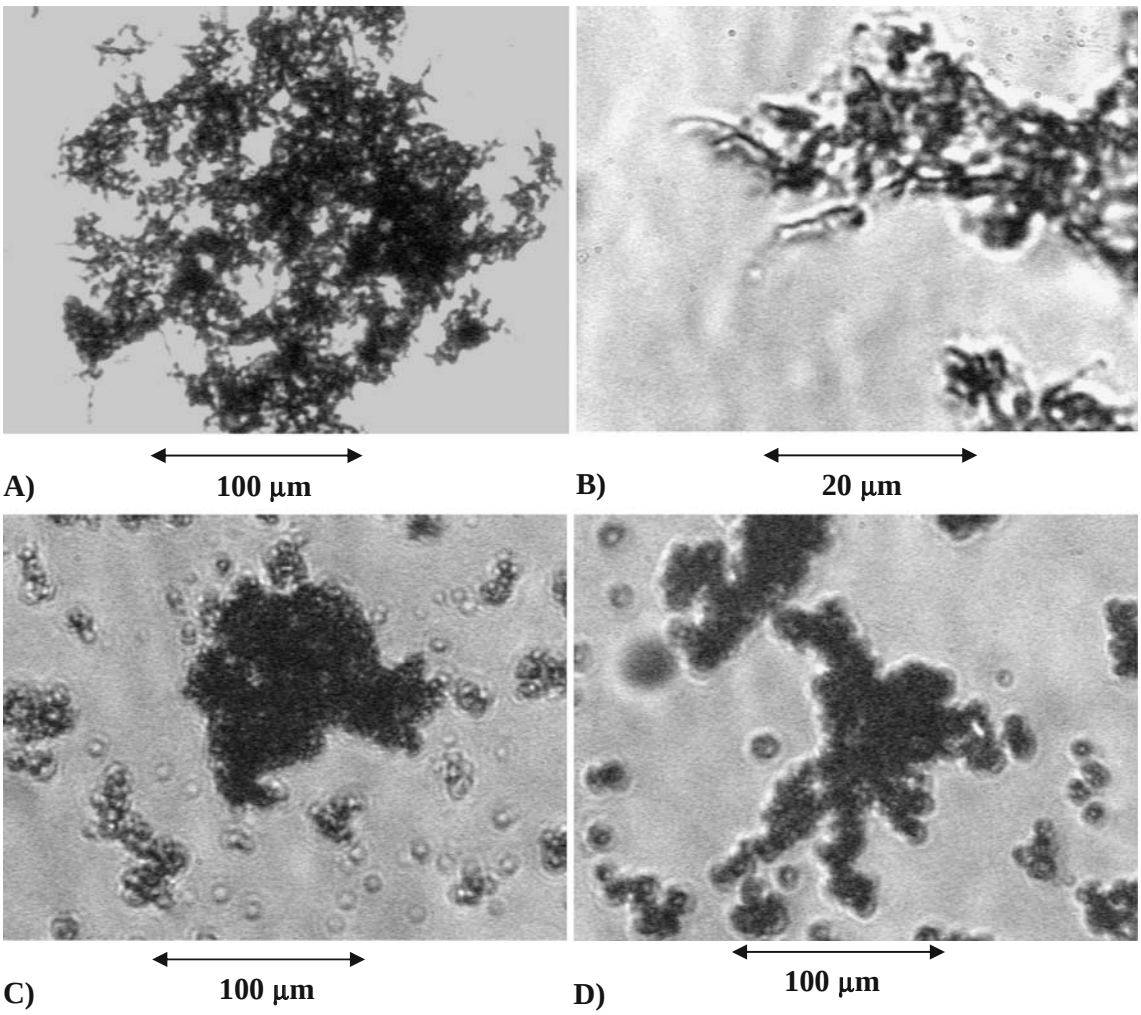

Fig. 4. Optical microscopy images of BSA particles suspended in HPFP with TFF particles magnified 10× (**A**) and 60× (**B**) after 30 s, wet milled BSA particles after 30 s at 10× (**C**) and spray dried BSA particles after 30 s at 10× (**D**). The flocs from TFF particles are more open than for wet milled and spray dried particles.

80% of the volume distribution between 100 nm and 1 μm (Fig. 9). The distributions nearly matched those of the original TFF particles in acetonitrile (Fig. 6).

In a third approach to analyze the TFF particle suspensions, the valve of the pMDI was submerged into acetonitrile and actuated. Submerging the actuator prevented the mixture of HFA droplets and particles from being exposed to ambient moisture and prevented HFA evaporation from effectively compacting the aerosolized particles. A slightly turbid dispersion was formed with an approximate particle concentration of 0.5 mg/mL, too low for detection by SLS, but not for DLS. From DLS, the particle size was 1–2 μm (Fig. 10) much smaller than the 250 μm floc size in HFA. Therefore, both the second and third approach indicate

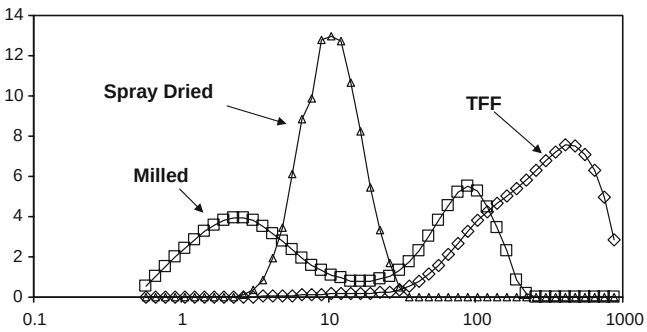

Fig. 5. Particle sizes in HPFP measured by static light scattering for BSA nanorods formed by TFF, cubes formed by wet milling and spheres by spray drying. The large particle size for TFF nanorods indicates flocculation, consistent with the microscopy results in Fig. 4.

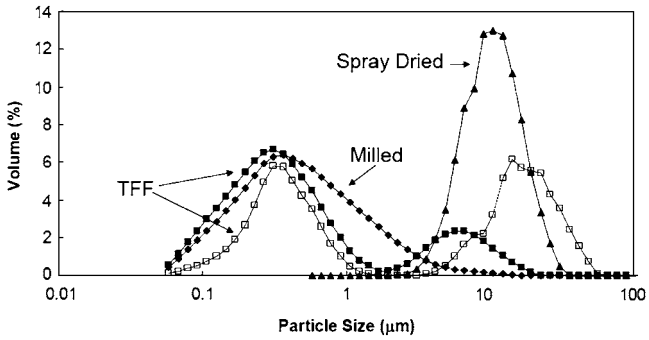

Fig. 6. Particle sizes in acetonitrile measured by static light scattering for BSA nanorods formed by thin film freezing (*TFF*), cubes formed by wet milling and spheres by spray drying. *Closed symbols* indicate sonicated powder and *open symbols* indicate unsonicated powder.

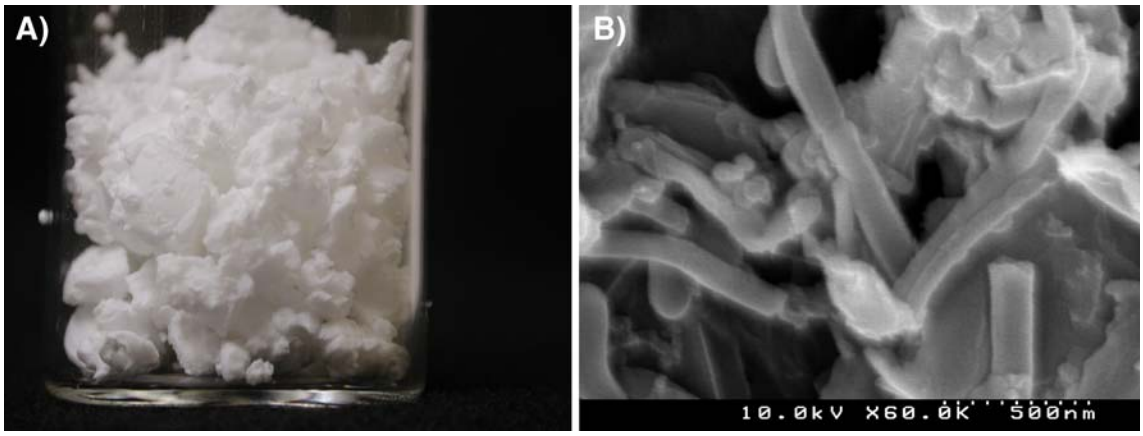

Fig. 7. TFF particles after suspension in ACN and lyophilization: photograph (**A**) and SEM (**B**).

the loosely flocculated nanorods in HFA may be broken up into primary nanorods, which will be shown to be beneficial for lung delivery.

Molecular Stability of BSA Exposed to HFA 227 as Determined by Optical Density

As a means to determine the molecular stability of BSA against forming aggregates in the HFA 227, the optical density (OD) of the BSA exposed to HFA 227 was measured. The HFA 227 was removed by cooling the HFA suspension to −80°C and allowing the HFA 227 to completely evaporate at atmospheric pressure. Aggregates of protein molecules did not appear to form according to OD measurements at 350 nm of 1 mg/mL BSA (27,57). The OD was the same at 0.042 for aqueous solutions in 10 mM phosphate pH=7.4 buffer prepared from bulk and TFF powder, both before and after storage in HFA 227 for 1 week. In the glassy state, BSA is less susceptible to aggregation (56,58). The total moisture to BSA content was 7% (*w*/*w*) for the suspended BSA particles in HFA 227 as determined by Karl–Fischer titration. Even at particle moisture contents of 8% (*w*/*w*), BSA glass transition temperatures T_g range between 80–100°C (59). Thus the temperature was well below T_g, assuming the HFA 227 did not contribute to plasticization.

Particle Characterization after Actuation Through the pMDI

The suspension must be stable for consistent dosing with a pMDI, which is commonly characterized by the dose (mass) delivered through the valve (DDV) (Table I). The concentration was 10 mg/mL or 0.7% (*w*/*w*) in each HFA suspension. Therefore, the theoretically delivered dose per actuation would be 1 mg with the 100 μL valve. For the BSA TFF particles, the DDV values were 92% and 63% of the theoretical delivery dose for the sonicated and unsonicated TFF particles, respectively (Table I). For the milled and spray dried suspensions with rapid settling, the DDV was only 30–31% of the theoretical loading. Here, the formulation was actuated less than 5 s after vigorous shaking. Therefore, these suspensions were not tested further for aerosol properties.

As shown in Table II and Fig. 11A and B, the d_a determined from the Anderson cascade impactor (ACI) and the Aerodynamic Particle Sizer (APS) were in good agreement and ranged from 3 to 4 μm, within the optimal 1–5 μm range for pulmonary delivery. As determined by the ACI, the fine particle fraction (FPF; particles less than 4.7 μm) was unusually high (35) for an HFA suspension, ranging from 38% to 47%, compared to 5% to 30% for typical suspensions (35), producing a fine particle dose/actuation of approximately 300 μg (Table I). The emitted dose (ED) (amount of drug

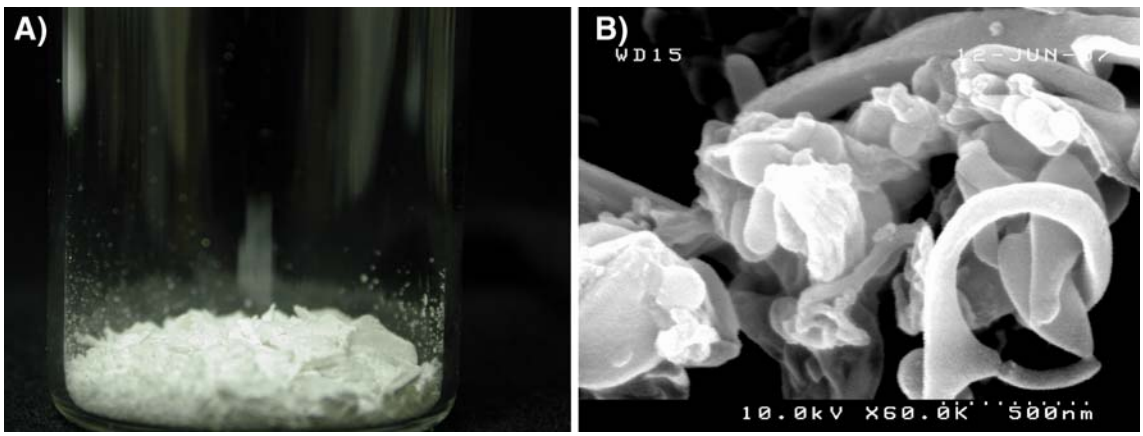

Fig. 8. Photograph (**A**) and SEM (**B**) of TFF particles after HFA 227 evaporation.

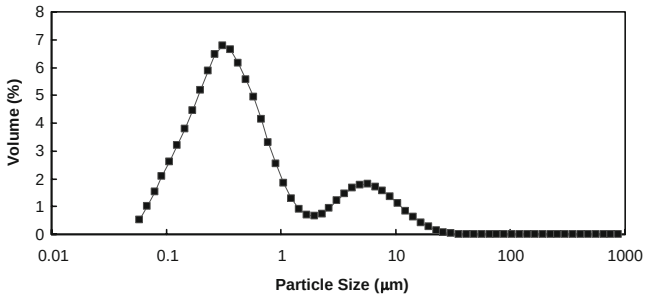

Fig. 9. Particle size distribution measured by static light scattering for BSA nanorods suspended in HFA 227 and transferred to acetonitrile and sonicated.

that exited the actuator) was approximately 70% of the DDV upon actuation (Table I and Fig. 11A).

The particles were recovered from the ACI for SEM analysis. The peak drug mass in the ACI was deposited on stages 3 and 4, with d_a between 2.0–4.7 μm (Fig. 11A). Therefore, particles were collected on stage 3 (d_a=3–4 μm). The particles were porous and composed of rods with diameters less than 500 nm (Fig. 12A, B), similar in morphology to the original nanorods in Fig. 2A.

The SEMs were analyzed by Scion software to determine the volume average diameter (60,61)

$$D_{\text{Vol}} = \frac{\sum d^4}{\sum d^3} \tag{3}$$

where d is the measured diameter of the particle. Approximately 200 of the BSA particles which consisted of aggregated nanorods were measured in 5 different images. The diameter of each particle was determined by averaging the longest and shortest diameter of each particle. The D_{vol} for BSA was approximately 9 μm (Table II). The d_g of the aerosolized particles were also measured by SLS. An effective refractive index n_e was calculated according to the Bruggeman mixing rule (62) based on the volume fraction of BSA in the aerosolized particle ϕ_g (Appendix). From the d_g and the d_a (Table II), the particle density ρ_g can be defined by (41)

$$d_a = d_g\sqrt{\rho_g} \tag{4}$$

where ρ_g=0.19 g/cm^3. The resulting $\phi_g = \rho_g/\rho_p = 0.14$. With n=1.45 and 1.00 for pure BSA and air, respectively, n_e=1.1. As shown in Table II the volume average $d(v,50)$ particle sizes varied by less than 1 μm from the values determined from the SEM micrographs. The consistent d_g values measured by SLS and SEM, and likewise for d_a, indicate that TFF particles form large porous particles, and with the optimal size range for pulmonary delivery upon aerosolization.

When the TFF particles were actuated above 10 mM phosphate buffer (pH=7.4) the particles were visually observed to dissolve in less than 5 s. The high surface area favors rapid dissolution, which could be advantageous for rapid dissolution rates of proteins that have low solubilities in water (6).

DISCUSSION

The attractive van der Waals forces play a key role in the floc formation, as depicted in the summary in Fig. 1 (14,45,63). According to the Derjaguin–Landau–Verwey–Overbeek (DLVO) theory, particle stability depends on counteracting the attractive van der Waals forces by electrostatic and/or steric repulsion (14,45,63). If attractive van der Waals (VdW) forces are dominant at all separation distances, particles flocculate and may then settle (14). Currently, electrostatic stabilization in HFAs is not well understood (11), but atomic force microscopy (AFM) measurements indicate that electrostatic forces may be negligible compared to attractive VdW forces (11,64). The understanding of steric stabilization in HFAs is in its infancy (36,39). While novel surfactants are being discovered, developed and approved (38,39), alternative means to form stable suspensions in HFAs without surfactants would be useful (11).

Suspension Stability for Porous or Hollow sphere Particles

The destabilizing van der Waals attractive forces between suspended particles are weaker for porous particles or hollow particles with thin solid shells (21,40). These particles can be stable for hours in HFAs, compared to non-porous 1–5 μm particles, which often flocculate and settle rapidly in less than 1 min (21,40) (see Fig. 2). Dellamary *et al.* (21) suggested that the increased suspension stability resulted from a weaker attractive VdW energy potential Φ_{vdw} between the particles, but quantitative calculations were not presented (11).

As shown in the Appendix the van der Waals energy Φ_{vdw} is directly proportional to the Hamaker constant A_{121}. In order to compare values of Φ_{vdw} it is necessary to choose a separation distance, h, between particles. Table III gives the h where Φ_{vdw} becomes equivalent to the thermal energy 3/2 k_BT at 298 K. An increase in h required to overcome thermal energy indicates stronger attraction between particles. In Table III, the porous particles with ϕ=0.5 had a calculated A_{121} (Eq. 11 in Appendix) that was nearly a factor of 4 lower than for the non-porous particles. Consequently, h was a factor of 3 smaller. The hollow spheres from TEM images (21) were estimated to have 2–5 μm diameters and ~100 nm thick shells. Although the A_{121} for the hollow sphere particles with solid shells was the same as for the non-porous particles, the calculated h was still lower by a factor of 2 as a consequence of the differences in the geometries (Eq. 14 in Appendix). Therefore, the Φ_{vdw} calculations quantify the benefits of weaker attraction for porous particles or for particles with hollow cores. A reduction in Φ_{vdw} or in h to overcome thermal energy can reduce the rate of flocculation over orders of magnitude as described by the stability ratio (45,63,65).

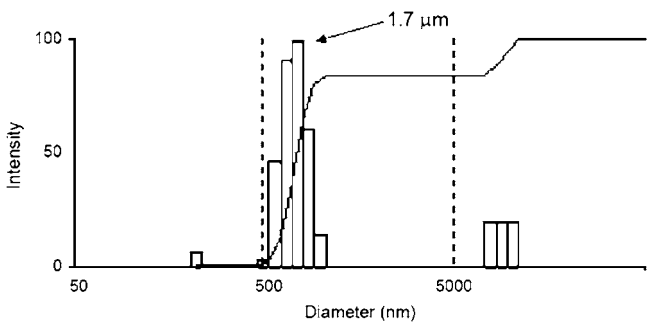

Fig. 10. DLS of TFF particles actuated through the pMDI valve submerged beneath acetonitrile.

Table I. Dosage and Aerodynamic Properties of Tff, Wet Milled, and Spray Dried Particle Suspensions in HFA 227

Formulation	DDV (μg)	%Theoretical DDV	FPF (%)	Fine Particle Dose/Actuation (μg)	ED (μg)
TFF BSA	915±21	92	47±4.0	318±31	695±133
TFF BSA unsonicated	625±95	63	–	–	–
Milled BSA	295±17	30	–	–	–
Spray dried BSA	308±38	31	–	–	–

Although, the porous or hollow sphere particles can effectively prevent flocculation, the particles are still subject to settling by gravity (11,21). If porous or hollow sphere BSA particles were suspended at ϕ_v=0.0077, the particles would occupy ~10% of the suspension and could potentially settle into a dense sediment. As shown in Table IV, the calculated settling rate for a single hollow sphere particle with a solid shell is 6.4×10^{-4} mm/s indicating that the particles would settle a distance of 2 cm in ~9 h. The settled particles would then potentially aggregate irreversibly leading to decreased FPFs upon aerosolization (34).

Flocculation of TFF Rods

To understand the space filling nature of the flocs composed of TFF rods, the volume fraction of the particles in the floc, ϕ_f, was calculated with Eq. 2. The volume of a TFF cylindrical rod, V_p=0.019 μm^3, was calculated from the equivalent volume of a sphere with particle diameter $d(v,50)$= 0.33 μm, which was measured by SLS (Fig. 6) in acetonitrile. For a rod with volume $V_p = \pi \cdot D^2 L/4$ and D=0.10 μm (Fig. 2A, B), L is determined as 2.4 μm and thus r=24. For r ~20, the predicted ϕ_f in Eq. 2 is ~1 order of magnitude lower than for spherical particles with equivalent d^{floc}, D_f, and where d_p for spheres scales as $V_p^{1/3}$ for rods.

To determine the effect of D_f on ϕ_f, the density of a floc ρ_f and ϕ_f were also determined experimentally from the visually observed floc settling rate, U_f, according to Stoke's law (66,67)

$$U_f = \frac{d^{floc^2} \cdot (\rho_f - \rho_L) \cdot g}{18 \cdot \mu} \quad (5)$$

where ρ_L and μ are the liquid density and viscosity, respectively, and d^{floc}=250 μm for TFF flocs and 100 μm for spray dried and milled flocs (Fig. 6). After solving for ρ_f in Eq. 5, ϕ_f may be determined by the straightforward material balance $\rho_f = \rho_L + \phi_f \cdot (\rho_p - \rho_L)$ (66,67). As seen in Table IV, ϕ_f for the TFF particles is 1–2 orders of magnitude lower than for the cube and spherical wet milled and spray dried particles. From Eqs. 1 and 2 the calculated D_f values are in a narrow range from 2.5 to 2.6 in each case. Although the milled and TFF particles have nearly equivalent d^{floc} and D_f values (Table IV), the 1/r scaling in Eq. 2 for rods accounts for the 1 order of magnitude decrease in ϕ_f, for a given V_p, which is consistent with the theoretical prediction above.

As illustrated in Fig. 1B, the open nanorod flocs with low ϕ_f filled large amounts of space in HFA and stacked upon each other like tumbleweeds to prevent settling. The volume fraction of flocs in the HFA suspension, ϕ^{flocs}, is given by $\phi^{flocs}=\phi_v/\phi_f$ (derivation given in Appendix) where ϕ^{flocs} determines the space filling capability of the flocs. As ϕ^{flocs} approaches 1 the flocs occupy the entire volume of HFA (Fig. 1B). For the dilute ϕ_v=0.00077 suspension (Fig. 3B), the calculated ϕ^{flocs} was 0.38 (Table IV) in good agreement with Fig. 3B. At a loading 10 fold higher, ϕ_v=0.0077, the entire vial was white without the appearance of spaces between flocs (Fig. 3A), as expected from the low ϕ_f. Here it was not possible to observe a settling rate as the visual appearance did not change for 1 year, the maximum time tested, as the ϕ^{flocs} of essentially unity prevented settling. In order for the cubic or spherical particles to produce ϕ^{flocs}=1 the required mass loadings for the milled and spray dried particles would be 6.7% (*w*/*w*) and 33% (*w*/*w*), respectively, compared to <0.7% (*w*/*w*) for the TFF rods. In contrast to the TFF rods, the hollow sphere particles would settle the length of the vial (~2 cm) by gravity in ~9 h according to Stoke's law (21) for a particle diameter of 5 μm and shell thickness of 100 μm. In the settled state with a high particle volume fraction and contact between protein chains they are more likely to form irreversible particle aggregates by interparticle diffusion and sintering (68).

The open flocs in HFA 227, that gave the stable suspensions, may be shown to be favored by the relatively strong attractive forces between the primary particles (45,63). At first, this may seem counterintuitive to the normal goal of lowering attractive forces to stabilize colloidal dispersions. Upon addition of the HFA, the relatively strong attractive forces between the primary rods, Φ_{vdw}, cause sticky collisions to "lock in" the open structure rapidly to inhibit collapse of the flocs (45,69). For weaker attractive forces between primary particles, collapse has been shown to be more prevalent as particles sample a greater number of energetically favorable locations to reduce the interfacial surface area (45,69). Therefore, rapid flocculation from sticky collisions facilitates the formation of low density flocs that fill the entire vial and prevent settling.

In contrast to the flocs in HFA 227, colloidal dispersions of primary TFF rods in acetonitrile settled in 3 days (Fig. 3F).

Table II. Aerodynamic Particle Sizes Determined by ACI And APS and Geometric Particle Sizes Determined by Laser Diffraction and SEM for TFF particles of BSA

ACI MMAD (μm)	ACI GSD	APS MMAD (μm)	APS GSD	d(v,50) Particle Diameter (μm)	SEM Particle Diameter (μm)	ρ_g (g/cm^3)
3.1±0.1	1.9±0.1	3.2±0.03	1.6±0.01	9.1±0.9	9.4	0.19

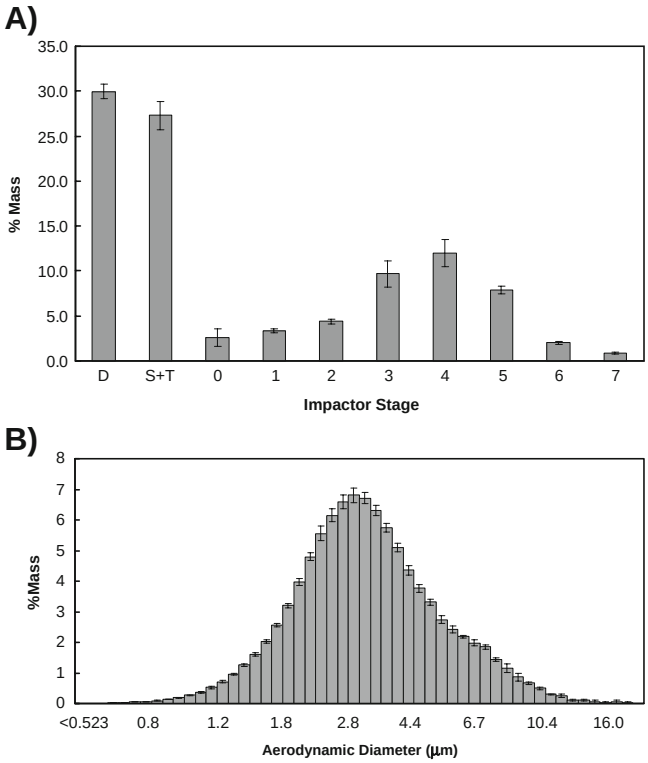

Fig. 11. ACI mass deposition profiles for device (*D*) and spacer and throat (*S+T*) and stages 0–7 (**A**), and APS mass distribution (**B**) for TFF BSA.

This settling rate agreed with the predicted settling rate of individual effective spheres with a diameter of 330 nm from light scattering given in Table IV. From Table III, the calculated A_{121} values for BSA in acetonitrile are 1 order of magnitude lower than in HFA 227 (Table III). Therefore, the stronger attractive forces between particles in HFA relative to ACN, favors formation of open flocs, resulting in more stable suspensions against settling.

Aerosol Formation from Stable Suspensions

Although the 250 µm flocs form stable suspensions, they are too large to produce optimal d_a. The shear forces in the actuator are needed to break apart the flocs. The calculation of these shear forces is rarely reported because the turbulence from the immediate onset of HFA evaporation produces complex cavitation events (61,70). According to empirical models, aerosolized HFA droplets are typically 10–30 µm in diameter (70). Thus we choose an HFA droplet diameter of 25 µm. Our hypothesis is that the attractive van der Waals interactions between primary particles within a floc are very weak such that the HFA droplets may template the 250 µm flocs into 25 µm subdomains with the same ϕ_f=0.0020 as illustrated schematically in Fig. 1.

To separate the subdomain from the floc the attractive forces between the interacting particles within (r_1) and outside (r_2) the subdomain surface (r_3) must be overcome (Fig. 13). The particle density within the floc was assumed to be uniform at 1.1×10^{17} m^{-3} as determined from the ϕ_f=0.0020 of the floc and V_p=0.019 µm^3 of the rod primary particle. The total number of interacting particles was assumed to occupy a 25 nm thick shell between r_1=12.488 µm and r_2=12.513 µm (Fig. 13). As shown in Table III, at separation distances greater than 25 nm the attractive energy between particles is similar to the thermal energy. This indicates that particles at separation distances >25 nm would not significantly contribute to the force necessary to separate the subdomain. The total number of particles in the shell was ~6, and therefore three particle–particle interactions had to be separated. The force to separate the interacting particles is dependent on the distance of separation of the particles (Eq. 13). An average separation distance between the interacting particles was determined as the difference of the geometric means determined by $<r_{13}> = (r_1 \cdot r_3)^{1/2}$ and $< r_{23} >= (r_2 \cdot r_3)^{1/2}$ as shown in Fig. 13 giving an average separation distance h between particles in the shell of 12.5 nm. From Eq. 13 the total force necessary to separate the subdomain from the floc is ~10^{-12} N (Eq. 13) assuming that the primary particle radius is 0.165 µm. The attractive force to separate the subdomain is very weak compared to the calculated shear force of ~10^{-4} N indicating that the subdomains can be easily templated by HFA droplets. The shear force, F_{shear}, on a 25 µm floc adhered to another floc was estimated by (71)

$$F_{shear} = \pi \cdot d^{floc^2} \cdot \tau = \frac{4 \cdot \pi \cdot d^{floc^2} \cdot \mu \cdot \nu^{\frac{7}{4}}}{\upsilon^{\frac{3}{4}} \cdot L_e^{\frac{1}{4}}} \quad (6)$$

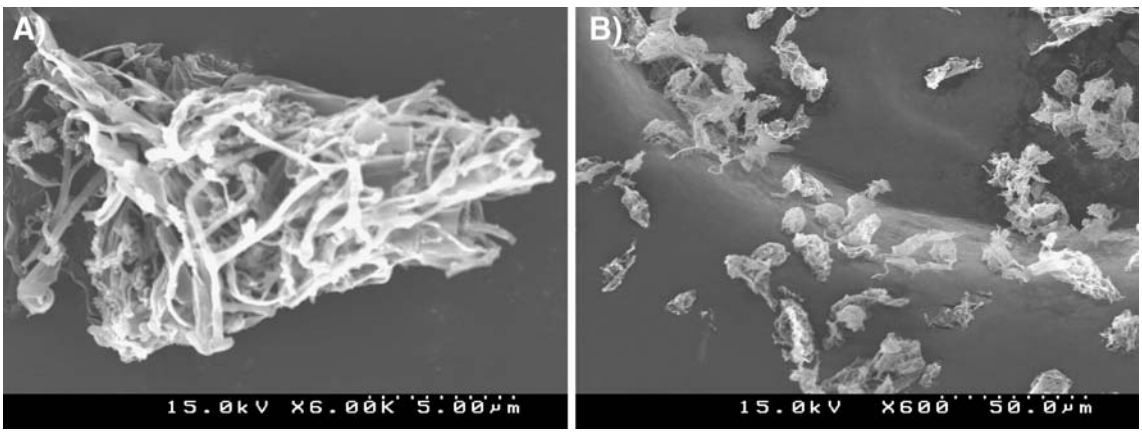

Fig. 12. BSA aerosol particles consisting of aggregates of nanorods collected from stage 3 of Anderson cascade impactor for BSA observed under high (**A**) and low magnification (**B**).

Table III. Calculation of the Van Der Waals (VdW) Interaction Potential Φ_{vdw} of BSA Particles in HFA 227

Particle Type	Particle Diameter (μm)	Hamaker Constant $10^{21}\times A_{121}$ (J)	Separation Distance (nm) at $\Phi_{vdw}=3/2k_BT$
Spray dried–non-porous	5.0	14	270
Spray dried–porous $\phi=0.50$	5.0	3.8	100
Spray dried–hollow sphere[a] $\phi_{shell}=1.0$	5.0	14	120
Spray dried–hollow sphere[a] $\phi_{shell}=0.50$	5.0	3.8	60
TFF nanorods	0.33	14	23
TFF nanorods[b]	0.33	2.6	6.9

[a] Shell thickness 100 nm
[b] TFF nanorods were in acetonitrile

where d^{floc} is the floc diameter, τ is the viscous stress, μ and υ are the viscosity and kinematic viscosity of HFA 227 in the liquid state at 25°C, respectively, v is the HFA droplet velocity during atomization, and L_e is the dimension of the largest eddy generated during pMDI atomization (approximated as the dimension of the turbulent flow cavity). The floc subdomains were estimated to be 25 μm in diameter, the size of an HFA 227 droplet. The viscosity and kinematic viscosity of HFA 227 were 2.44×10^{-4} Pa·s and 1.76×10^{-7} m^2/s, respectively (14). The velocity of the HFA droplets during atomization was estimated to be 30 m/s (61), and L_e was 0.7 mm, the pMDI valve diameter.

The concept of templating of the 25 μm subdomains is supported by a material balance on the protein between the volume of the HFA droplet, V_{HFA}, and the volume of the dry aerosolized particle, V_g, (Fig. 1B) given by

$$V_g \cdot \rho_g = V_{HFA} \cdot \rho_{HFA} \tag{7}$$

where BSA concentrations are given by $\rho_{HFA} = \phi_v \cdot \rho_p$, and $\rho_g = \phi_g \cdot \rho_p$. It is assumed that the volume fraction of particles in a HFA droplet is approximately equal to ϕ_v as a result of the break up of the flocs. Because of the high ϕ^{flocs} (Figs. 1B and 3A), it is expected that most of the HFA droplets are likely to be filled with a subdomain. From the measured d_g and d_a in Table II and $\rho_g=0.19$ g/cm^3 (Eq. 4), $\phi_g=0.14$. The ϕ_g is nearly 20 times greater than ϕ_v in the vial. Therefore, the capillary forces in the shrinking HFA droplets during evaporation collapse the flocs (33). Eq. 7 is refined to relate ϕ_g to ϕ_v as

$$\phi_g \cdot d_g^3 = \frac{f_{BSA}}{f_{HFA}} \cdot \phi_v \cdot d_{HFA}^3 \tag{8}$$

where d is a diameter, $f_{BSA}=0.7$ accounts for the mass fraction of drug that is emitted from the actuator, and $f_{HFA}=0.5$ accounts for the mass fraction of HFA that exits the actuator orifice to form aerosolized liquid droplets (relative to vapor) (61).

From Eq. 8 with $d_g=9.3$ μm (Table II), $d_{HFA}=25$ μm (70), and $\phi_v=0.0077$, the calculated $\phi_g=0.21$, which compares reasonably well to the experimentally determined $\phi_g=0.14$. Also the polydispersity in the aerodynamic properties was small. It would be unlikely that any other factor besides templating of the flocs with relatively uniform HFA droplets could explain these low polydispersities.

The control experiment in Fig. 8A supports this argument since the TFF particles remained below the meniscus of the evaporating HFA 227. The tapped density of the particles was approximately 0.10 g/cm^3 (Fig. 8A) which is within a factor of 2 of the calculated density (0.19 g/cm^3) of the aerosolized particle. Therefore, the capillary forces acting on the TFF particles during HFA evaporation compacted the particles into denser aggregates with a highly desirable value of the d_a. If needed, the d_a may be manipulated further by varying the valve volume and geometry and the HFA droplet generation. If the particles had not collapsed partially, they would have been too large and light for pulmonary delivery. Even after this collapse, the porosity and surface area were still relatively high and favorable for high dissolution rates of small molecules and proteins with limited solubilities, relative to nonporous particles (6).

CONCLUSIONS

High (38–47%) fine particle fractions in HFA 227 pMDI delivery were achieved with flocculated BSA nanorods stable against settling for up to 1 year, without the use of surfactants and cosolvents. Analysis of experimental settling rates of dilute suspensions indicated that the volume fraction, ϕ_f, of the nanorods in the flocs was an order of magnitude lower than for flocs of spherical particles produced by wet milling or spray drying. The rapid and sticky attractive collisions of nanorods facilitates the formation of low density flocs (250 μm) which stack upon each other to fill the entire solvent volume to prevent settling (Fig. 1B). In contrast, denser flocs of spherical particles filled much less space and rapidly settled within 60 s (Fig. 1A). The novel concept of

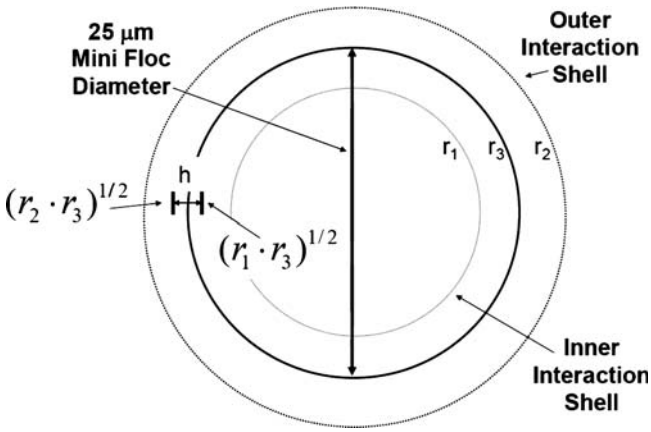

Fig. 13. Diagram of subdomain with radius r_3 held within a floc by particles interacting within shells of radius r_1 and r_2.

Table IV. Settling Behavior of BSA Particles Prepared by TFF, Wet Milling, and Spray Drying and Calculations for Porous Shell Particles Prepared by Spray Drying

Particle Type	d_p (μm)	d^{floc} (μm)	$(\rho_L-\rho_f)$ (g/cm^3)	U_f (mm/s)	U_p (mm/s)	ϕ_v	ϕ^{flocs}	ϕ_f	D_f
TFF	0.33[a]	250	0.00022	0.023	2.4×10^{-5}	0.00077	0.38	0.0020	2.5
Milled	0.41	100	0.0080[b]	0.13	3.7×10^{-5}	0.0067	0.11	0.073	2.5
Spray dried	6.3	100	0.040	0.80	8.8×10^{-3}	0.0077	0.021	0.36	2.6
Spray dried–hollow sphere	5.0[c]	–	0.013[d]	–	6.4×10^{-4}	–	–	–	–

[a] Value determined from the equivalent volume of a sphere measured from laser light scattering
[b] The density difference was determined by $\rho_f-\rho_L$ with ρ_p=1.5 g/cm^3
[c] Determined from dimensions given by Dellamary *et al.* (21)
[d] Calculated for primary particle with 100 nm thick shell

purposely flocculating nanorods to prevent settling is fundamentally opposite the conventional approach of stabilizing colloidal dispersions of pre-formed primary particles with surfactants.

The reversibility of the nanorod flocs in HFA 227 was demonstrated by break-up of the flocs into individual 330 nm primary rod particles upon transfer to the more polar solvent acetonitrile.

A material balance on a shrinking HFA droplet containing a 25 μm floc subdomain predicts a final volume fraction of BSA in the aerosolized particle in agreement with experiment. Therefore, the attractive van der Waals interactions between primary particles within the floc are sufficiently weak such that the atomized HFA droplets initially template the 250 μm flocs into 25 μm subdomains. The aerosolized particles with a d_a of 3–4 μm and d_g of ~10 μm are optimal for high fine particle fractions via a pMDI. The concept of forming open flocs composed of aymmetric particles, for example nanorods, that are stable against settling without surfactants, and templating the flocs to achieve optimal d_as and high FPFs is of practical interest for wide classes of low and high molecular weight pharmaceuticals and biopharmaceuticals (29,72,73).

ACKNOWLEDGEMENTS

This material is supported in part by the STC Program of the National Science Foundation under Agreement No. CHE987664, the Robert A. Welch Foundation, and the Process Science and Technology Center at the University of Texas. The authors also wish to thank TSI for access to the APS 3321.

APPENDIX

Bruggeman mixing rule

For porous particles or suspensions with a BSA particle volume fraction ϕ, the effective refractive index n_e and dielectric constant ε_e can be calculated from the following Bruggeman mixing relationships

$$(1-\phi)\frac{n_A^2-n_e^2}{n_A^2+2n_e^2}+\phi\frac{n_B^2-n_e^2}{n_B^2+2n_e^2}=0 \tag{9}$$

$$(1-\phi)\frac{\varepsilon_A-\varepsilon_e}{\varepsilon_A+2\varepsilon_e}+\phi\frac{\varepsilon_B-\varepsilon_e}{\varepsilon_B+2\varepsilon_e}=0 \tag{10}$$

where ϕ can be either ϕ_g or ϕ_f, the subscript A denotes air or HFA 227, and B denotes BSA.

Attractive van der Waals equations

The Φ_{vdw} is directly proportional to the Hamaker constant A_{121} for one particle interacting with another (subscript 1) across solvent, such as HFA 227 or acetonitrile, (subscript 2) as a function of the particle geometry (74). The Hamaker constant A_{121} may be approximated by

$$A_{121}=\left(\sqrt{A_{11}}-\sqrt{A_{22}}\right)^2 \tag{11}$$

where A_{11} and A_{22} are the pure Hamaker constants for BSA and the suspending media interacting across a vacuum, respectively. These values were calculated from Lifshitz theory (74,75). To determine A_{11} for porous BSA particles in HFA 227, ε_e and n_e were calculated with the Bruggeman mixing rule (Eqs. 9 and 10) at ϕ=0.5 in HFA 227 (40,62). The van der Waals attractive potential between identical spherical particles (74)

$$\Phi_{vdw}=-\frac{A_{121}R}{12h} \tag{12}$$

which has an attractive force F_{vdw} given as

$$F_{vdw}=\frac{A_{121}R}{12h^2} \tag{13}$$

where R is the spherical particle radius and h is the separation distance between the particle surfaces and for identical hollow spheres with solid shells (76)

$$\Phi_{vdw}=-\frac{A_{121}R}{12}\left(\frac{1}{h+2t}-\frac{2}{h+t}+\frac{1}{h}\right)-\frac{A_{121}}{6}\times\ln\left(\frac{h(h+2t)}{(h+t)^2}\right) \tag{14}$$

where t is the shell thickness. For identical rods, E_{vdw} can be calculated for parallel

$$\Phi_{vdw}=-\frac{A_{121}LR^{1/2}}{24h^{3/2}} \tag{15}$$

or crossed cylinders

$$\Phi_{vdw}=-\frac{A_{121}R}{6h} \tag{16}$$

where L is the cylinder length. The values from Eq. 15 and 16 were averaged to give equal weight to the two orientations (Table III).

Space filling floc derivation

A vial filled with protein particles of total mass m and primary particle density ρ_p into a given volume V of HFA 227 has a volume fraction ϕ_v defined as

$$\phi_v = \frac{m/\rho_p}{V} \tag{17}$$

The volume fraction of particles in a floc ϕ_f is

$$\phi_f = \frac{V_p \cdot k}{V_f} \tag{18}$$

where V_p and V_f are the volume of a spherical primary particle and a spherical floc, respectively, and k is the number of primary particles in a floc.

The volume fraction of flocs in HFA ϕ^{flocs} is defined as

$$\phi^{flocs} = \frac{V_f \cdot N_f}{V} \tag{19}$$

where N_f is the total number of flocs in suspension. $N_f = N_p/k$ where $N_p = m/m_p$ is the total number of primary particles in suspension and $m_p = V_p \cdot \rho_p$ is the mass of a primary particle. Substitution into Eq. 19 gives

$$\phi^{flocs} = \frac{V_f \cdot m}{V_p \cdot k \cdot V \cdot \rho_p} = \frac{\phi_v}{\phi_f} \tag{20}$$

REFERENCES

1. R. U. Agu, M. I. Ugwoke, M. Armand, R. Kinget, and N. Verbeke. The lung as a route for systemic delivery of therapeutic proteins and peptides. *Respir. Res.* **2**:198–209 (2001) doi:10.1186/rr58.
2. A. L. Adjei, and P. K. Gupta. *Inhalation delivery of therapeutic peptides and proteins*. *Int. J. Pharm*. **159**:259 (1997).
3. S. White, D. B. Bennett, S. Cheu, P. W. Conley, D. B. Guzek, S. Gray, J. Howard, R. Malcolmson, J. M. Parker, P. Roberts, N. Sadrzadeh, J. D. Schumacher, S. Seshadri, G. W. Sluggett, C. L. Stevenson, and N. J. Harper. EXUBERA: pharmaceutical development of a novel product for pulmonary delivery of insulin. *Diabetes Technol. Ther.* **7**:896–906 (2005) doi:10.1089/dia.2005.7.896.
4. S. A. Shoyele, and A. Slowey. Prospects of formulating proteins/peptides as aerosols for pulmonary drug delivery. *Int. J. Pharm.* **314**:1–8 (2006) doi:10.1016/j.ijpharm.2006.02.014.
5. H. M. Courrier, N. Butz, and T. F. Vandamme. Pulmonary drug delivery systems: recent developments and prospects. *Crit. Rev. Ther. Drug Carr. Syst.* **19**:425–498 (2002) doi:10.1615/CritRevTherDrugCarrierSyst.v19.i45.40.
6. M. J. Kwon, J. H. Bae, J. J. Kim, K. Na, and E. S. Lee. Long acting porous microparticle for pulmonary protein delivery. *Int. J. Pharm.* **333**:5–9 (2007) doi:10.1016/j.ijpharm.2007.01.016.
7. J. S. Patton, and P. R. Byron. Inhaling medicines: delivering drugs to the body through the lungs. *Nature Reviews Drug Discovery*. **6**:67–74 (2007) doi:10.1038/nrd2153.
8. V. Codrons, F. Vanderbist, R. K. Verbeeck, M. Arras, D. Lison, V. Preat, and R. Vanbever. Systemic delivery of parathyroid hormone (1–34) using inhalation dry powders in rats. *J. Pharm. Sci.* **92**:938–950 (2003) doi:10.1002/jps.10346.
9. L. Garcia-Contreras, and H. D. C. Smyth. Liquid-spray or dry-powder systems for inhaled delivery of peptide and proteins? *American Journal of Drug Delivery*. **3**:29–45 (2005) doi:10.2165/00137696-200503010-00004.
10. D. Traini, P. Young, P. Rogueda, and R. Price. The use of AFM and surface energy measurements to investigate drug–canister material interactions in a model pressurized metered dose inhaler formulation. *Aerosol Sci. Tech.* **40**:227–236 (2006) doi:10.1080/02786820500543316.
11. P. Rogueda. Novel hydrofluoroalkane suspension formulations for respiratory drug delivery. *Expert Opinion on Drug Delivery*. **2**:625–638 (2005) doi:10.1517/17425247.2.4.625.
12. R. O. Williams III, and J. Liu. Formulation of a protein with propellant HFA 134a for aerosol delivery. *Eur. J. Pharm. Sci.* **7**:137–144 (1999) doi:10.1016/S0928-0987(98)00015-3.
13. R. O. Williams III, M. Repka, and J. Liu. Influence of propellant composition on drug delivery from a pressurized metered-dose inhaler. *Drug Dev. Ind. Pharm.* **24**:763–770 (1998) doi:10.3109/03639049809082724.
14. K. A. Johnson. Interfacial phenomena and phase behavior in metered dose inhaler formulations. In A. J. Hickey (ed.), *Inhalation Aerosols: Physical and Biological Basis for Therapy*, Vol. 221. Lung Biology in Health and Disease, 2007.
15. E. A. Quinn, R. T. Forbes, A. C. Williams, M. J. Oliver, L. McKenzie, and T. S. Purewal. Protein conformational stability in the hydrofluoroalkane propellants tetrafluoroethane and heptafluoropropane analyzed by Fourier transform Raman spectroscopy. *Int. J. Pharm.* **186**:31–41 (1999) doi:10.1016/S0378-5173(99)00135-0.
16. M. J. Oliver, L. McKenzie, W. D. Graffiths, G. R. Morgan, and N. O'Kelly. Initial assessment of a protein formulated in pressurized MDIS for pulmonary delivery. In *RDD VII*, 2000.
17. C. Benfait. Kos reports achievement of new research and development milestones. *Kos Press Release* (2004).
18. J. Heyder, J. Gebhart, G. Rudolf, C. F. Schiller, and W. Stahlhofen. Deposition of particles in the human respiratory tract in the size range 0.005–15 μm. *J. Aerosol Sci.* **17**:811–825 (1986) doi:10.1016/0021-8502(86)90035-2.
19. A. Ben-Jebria, D. Chen, M. L. Eskew, R. Vanbever, R. Langer, and D. A. Edwards. Large porous particles for sustained protection from carbachol-induced bronchoconstriction in guinea pigs. *Pharm. Res.* **16**:555–561 (1999) doi:10.1023/A:1018879331061.
20. N. Tsapis, D. Bennett, B. Jackson, D. A. Weitz, and D. A. Edwards. Trojan particles: large porous carriers of nanoparticles for drug delivery. *Proc. Natl. Acad. Sci. U. S. A.* **99**:12001–12005 (2002) doi:10.1073/pnas.182233999.
21. L. A. Dellamary, T. E. Tarara, D. J. Smith, C. H. Woelk, A. Adractas, M. L. Costello, H. Gill, and J. G. Weers. Hollow porous particles in metered dose inhalers. *Pharm. Res.* **17**:168–174 (2000) doi:10.1023/A:1007513213292.
22. Y.-F. Maa, P.-A. Nguyen, T. Sweeney, S. J. Shire, and C. C. Hsu. Protein inhalation powders: spray drying *vs* spray freeze drying. *Pharm. Res.* **16**:249–254 (1999) doi:10.1023/A:1018828425184.
23. Y.-F. Maa, and H. R. Costantino. Spray freeze-drying of biopharmaceuticals: applications and stability considerations. In H. R. Costantino, and M. J. Pikal (eds.), *Biotechnology: Pharmaceutical Aspects. 2. Lyophilization of Biopharmaceuticals, Vol. 2*, American Association of Pharmaceutical Scientists, Arlington, 2004, pp. 519–561.
24. Z. Yu, A. S. Garcia, K. P. Johnston, and R. O. Williams III. Spray freezing into liquid nitrogen for highly stable protein nanostructured microparticles. *Eur. J. Pharm. Biopharm.* **58**:529–537 (2004) doi:10.1016/j.ejpb.2004.04.018.
25. J. D. Engstrom, D. T. Simpson, E. Lai, R. O. Williams III, and K. P. Johnston. Morphology of protein particles produced by spray freezing of concentrated solutions. *Eur. J. Pharm. Biopharm.* **65**:149–162 (2007) doi:10.1016/j.ejpb.2006.08.005.
26. J. D. Engstrom, D. T. Simpson, C. Cloonan, E. Lai, R. O. Williams III, G. B. Kitto, and K. P. Johnston. Stable high surface area lactate dehydrogenase particles produced by spray freezing into liquid nitrogen. *Eur. J. Pharm. Biopharm.* **65**:163–174 (2007) doi:10.1016/j.ejpb.2006.08.002.
27. Z. Yu, K. P. Johnston, and R. O. Williams III. Spray freezing into liquid *versus* spray-freeze drying: Influence of atomization on

protein aggregation and biological activity. *Eur. J. Pharm. Sci.* **27**:9–18 (2006) doi:10.1016/j.ejps.2005.08.010.
28. Z. Yu, T. L. Rogers, J. Hu, K. P. Johnston, and R. O. Williams III. Preparation and characterization of microparticles containing peptide produced by a novel process: spray freezing into liquid. *Eur. J. Pharm. Biopharm.* **54**:221–228 (2002) doi:10.1016/S0939-6411(02)00050-4.
29. J. D. Engstrom, E. S. Lai, B. Ludher, B. Chen, T. E. Milner, G. B. Kitto, R. O. Williams III, and K. P. Johnston. Formation of stable submicron protein particles by thin film freezing. *Pharm. Res.* **25**:1334–1346 (2008) doi:10.1007/s11095-008-9540-4.
30. S. D. Webb, S. L. Golledge, J. L. Cleland, J. F. Carpenter, and T. W. Randolph. Surface adsorption of recombinant human interferon-γ in lyophilized and spray-lyophilized formulations. *J. Pharm. Sci.* **91**:1474–1487 (2002) doi:10.1002/jps.10135.
31. X. C. Nguyen, J. D. Herberger, and P. A. Burke. Protein powders for encapsulation: a comparison of spray-freeze drying and spray drying of darbepoetin alfa. *Pharm. Res.* **21**:507–514 (2004) doi:10.1023/B:PHAM.0000019306.89420.f0.
32. Y.-F. Maa, and S. J. Prestrelski. Biopharmaceutical powders: particle formation and formulation considerations. *Curr. Pharm. Biotechnol.* **1**:283–302 (2000) doi:10.2174/1389201003378898.
33. I. Gonda. Development of a systematic theory of suspension inhalation aerosols. I. A framework to study the effects of aggregation on the aerodynamic behavior of drug particles. *Int. J. Pharm.* **27**:99–116 (1985) doi:10.1016/0378–5173(85)90189-9.
34. Y.-H. Liao, M. B. Brown, S. A. Jones, T. Nazir, and G. P. Martin. The effects of polyvinyl alcohol on the *in vitro* stability and delivery of spray-dried protein particles from surfactant-free HFA 134a-based pressurised metered dose inhalers. *Int. J. Pharm.* **304**:29–39 (2005) doi:10.1016/j.ijpharm.2005.07.013.
35. M. Keller. Innovations and perspectives of metered dose inhalers in pulmonary drug delivery. *Int. J. Pharm.* **186**:81–90 (1999) doi:10.1016/S0378-5173(99)00132-5.
36. C. Vervaet, and P. R. Byron. Drug-surfactant-propellant interactions in HFA-formulations. *Int. J. Pharm.* **186**:13–30 (1999) doi:10.1016/S0378-5173(99)00134-9.
37. F. E. Blondino, and P. R. Byron. Surfactant dissolution and water solubilization in chlorine-free liquified gas propellants. *Drug Dev. Ind. Pharm.* **24**:935–945 (1998) doi:10.3109/03639049809097273.
38. R. P. S. Peguin, P. Selvam, and S. R. P. da Rocha. Microscopic and thermodynamic properties of the HFA134a-water interface: atomistic computer simulations and tensiometry under pressure. *Langmuir.* **22**:8826–8830 (2006) doi:10.1021/la0608157.
39. L. Wu, R. P. S. Peguin, P. Selvam, U. Chokshi, and S. R. P. da Rocha. Molecular scale behavior in alternative propellant-based inhaler formulations. In A. J. Hickey (ed), *Inhalation Aerosols: Physical and biological basis for therapy*, Vol. 221. Lung Biology in Health and Disease, 2007.
40. R. Vanbever, J. D. Mintzes, J. Wang, J. Nice, D. Chen, R. Batycky, R. Langer, and D. A. Edwards. Formulation and physical characterization of large porous particles for inhalation. *Pharm. Res.* **16**:1735–1742 (1999) doi:10.1023/A:1018910200420.
41. D. A. Edwards, J. Hanes, G. Caponetti, J. Hrkach, A. Ben-Jebria, M. L. Eskew, J. Mintzes, D. Deaver, N. Lotan, and R. Langer. Large porous particles for pulmonary drug delivery. *Science*. **276**:1868–1871 (1997) doi:10.1126/science.276.5320.1868.
42. J. Tam, J. T. McConville, R. O. Williams III, and K. P. Johnston. Amorphous cyclosporin A nanodispersions for enhanced pulmonary deposition and dissolution. *J. Pharm. Sci.* in press (2008) doi:10.1002/jps.21367.
43. Z. Jiang, and Y. Guan. Flocculation morphology: effect of particulate shape and coagulant species on flocculation. *Water Sci. Technol.* **53**:9–16 (2006) doi:10.2166/wst.2006.339.
44. I. Goodarz-Nia, and D. N. Sutherland. Floc simulation. Effects of particle size and shape. *Chem. Eng. Sci.* **30**:407–12 (1975) doi:10.1016/0009-2509(75)85005-6.
45. P. C. Hiemenz and R. Rajagopalan. *Principles of colloid and surface chemistry*, Marcel Dekker, New York, 1997.
46. A. P. Philipse, and A. M. Wierenga. On the density and structure formation in gels and clusters of colloidal rods and fibers. *Langmuir.* **14**:49–54 (1998) doi:10.1021/la9703757.
47. A. P. Philipse. The random contact equation and its implications for (colloidal) rods in packings, suspensions, and anisotropic powders. *Langmuir.* **12**:5971 (1996) doi:10.1021/la960869o.
48. R. G. Larson. *The structure and rheology of complex fluids*. Oxford University Press, New York, 1999.
49. P. G. Smith Jr., W. Ryoo, and K. P. Johnston. Electrostatically stabilized metal oxide particle dispersions in carbon dioxide. *J. Phys. Chem. B*. **109**:20155–20165 (2005) doi:10.1021/jp0532521.
50. Y. Kim, S. H. Atwell, and R. G. Bell. Determination of water in pressurized pharmaceutical metered dose aerosol products. *Drug Dev. Ind. Pharm.* **18**:2185–2195 (1992) doi:10.3109/03639049209038756.
51. R. O. Williams III, J. Liu, and J. J. Koleng. Influence of metering chamber volume and water level on the emitted dose of a suspension-based pMDI containing propellant 134a. *Pharm. Res.* **14**:438–443 (1997) doi:10.1023/A:1012087130114.
52. E. Berlin, and M. J. Pallansch. Densities of several proteins and L-amino acids in the dry state. *J. Phys. Chem.* **72**:1887–1889 (1968) doi:10.1021/j100852a004.
53. P. G. A. Rogueda. HPFP, a model propellant for pMDIs. *Drug Dev. Ind. Pharm.* **29**:39–49 (2003) doi:10.1081/DDC-120016682.
54. R. Ashayer, P. F. Luckham, S. Manimaaran, and P. Rogueda. Investigation of the molecular interactions in a pMDI formulation by atomic force microscopy. *Eur. J. Pharm. Sci.* **21**:533–543 (2004) doi:10.1016/j.ejps.2003.12.003.
55. D. Traini, M. Young Paul, P. Rogueda, and R. Price. *In vitro* investigation of drug particulates interactions and aerosol performance of pressurised metered dose inhalers. *Pharm. Res.* **24**:125–135 (2007) doi:10.1007/s11095-006-9130-2.
56. S. L. Nail, S. Jiang, S. Chongprasert, and S. A. Knopp. Fundamentals of freeze-drying. In S. L. Nailand, and M. J. Akers (eds.), *Pharmaceutical Biotechnology. 14. Development and Manufacture of Protein Pharmaceuticals, Vol. 14*, Kluwer, New York, 2002, pp. 281–360.
57. S. D. Webb, J. L. Cleland, J. F. Carpenter, and T. W. Randolph. A new mechanism for decreasing aggregation of recombinant human interferon-g by a surfactant: slowed dissolution of lyophilized formulations in a solution containing 0.03% polysorbate 20. *J. Pharm. Sci.* **91**:543–558 (2002) doi:10.1002/jps.10033.
58. J. F. Carpenter, B. S. Chang, W. Garzon-Rodriguez, and T. W. Randolph. Rational design of stable lyophilized protein formulations: theory and practice. In J. F. Carpenter, and M. C. Manning (eds.), *Pharmaceutical Biotechnology. 13. Rational Design of Stable Protein Formulations, Vol. 13*, Kluwer, New York, 2002, pp. 109–133.
59. A. Farahnaky, F. Badii, I. A. Farhat, J. R. Mitchell, and S. E. Hill. Enthalpy relaxation of bovine serum albumin and implications for its storage in the glassy state. *Biopolymers*. **78**:69–77 (2005) doi:10.1002/bip.20265.
60. B. Y. Shekunov, P. Chattopadhyay, H. H. Y. Tong, and A. H. L. Chow. Particle size analysis in pharmaceutics: principles, methods and applications. *Pharm. Res.* **24**:203–227 (2007) doi:10.1007/s11095-006-9146-7.
61. W. H. Finlay. *The mechanics of inhaled pharmaceutical aerosols*, Academic,New York, 2001.
62. A. Sihvola. *Electromagnetic mixing formulas and applications*, Institute of Electrical Engineers, London, 1999.
63. W. B. Russel, D. A. Saville, and W. R. Schowalter. *Colloidal dispersions*, Cambridge University Press, Cambridge, 1989.
64. D. Traini, P. Rogueda, P. Young, and R. Price. Surface Energy and Interparticle Forces Correlations in Model pMDI Formulations. *Pharm. Res.* **22**:816–825 (2005) doi:10.1007/s11095-005-2599-2.
65. M. A. Bevan. *Effect of adsorbed polymer on the interparticle potential, chemical engineering*. Carnegie Mellon University, Pittsburgh, 1999.
66. P. Tang, J. Greenwood, and J. A. Raper. A model to describe the settling behavior of fractal aggregates. *J. Colloid Interface Sci.* **247**:210–219 (2002) doi:10.1006/jcis.2001.8028.
67. C. Fargues, and C. Turchiuli. Structural characterization of flocs in relation to their settling performances. *Chem. Eng. Res. Des.* **82**:1517 (2004) doi:10.1205/cerd.82.11.1517.52026.

68. H. Abramowitz, P. S. Shah, P. F. Green, and K. P. Johnston. Welding colloidal crystals with carbon dioxide. *Macromolecules*. **37**:7316–7324 (2004) doi:10.1021/ma048961b.
69. D. R. Ulrich. Chemical processing of ceramics. *Chem. Eng. News*. **68**:28–40 (1990).
70. H. D. C. Smyth, A. J. Hickey, and R. M. Evans. Aerosol generation from propellant-driven metered dose inhalers. In J. Hickey Anthony (ed), *Inhalation Aerosols: Physical and Biological Basis for Therapy*, Vol. 221, Lung biology in health and disease, 2007, pp. 399–416.
71. D. L. French, D. A. Edwards, and R. W. Niven. The influence of formulation on emission, deaggregation and deposition of dry powders for inhalation. *J. Aerosol Sci.* **27**:769–783 (1996) doi:10.1016/0021-8502(96)00021-3.
72. T. L. Rogers, A. C. Nelsen, J. Hu, J. N. Brown, M. Sarkari, T. J. Young, K. P. Johnston, and R. O. Williams III. A novel particle engineering technology to enhance dissolution of poorly water soluble drugs: spray-freezing into liquid. *Eur. J. Pharm. Biopharm.* **54**:271–280 (2002) doi:10.1016/S0939-6411(02)00063-2.
73. T. L. Rogers, K. A. Overhoff, P. Shah, P. Santiago, M. J. Yacaman, K. P. Johnston, and R. O. Williams III. Micronized powders of a poorly water soluble drug produced by a spray-freezing into liquid-emulsion process. *Eur. J. Pharm. Biopharm.* **55**:161–72 (2003) doi:10.1016/S0939-6411(02)00193-5.
74. J. Israelachvili. *Intermolecular and surface forces*. Academic, San Diego, 1992.
75. S. Takashima. Proton fluctuation in protein. Experimental study of the Kirkwood–Shumaker theory. *J. Phys. Chem.* **69**:2281–2286 (1965) doi:10.1021/j100891a023.
76. R. Tadmor. The London–van der Waals interaction energy between objects of various geometries. *J. Phys. Condens. Matter.* **13**:L195–L202 (2001) doi:10.1088/0953-8984/13/9/101.